

A second-order consistent, low-storage method for time-resolved channel flow simulations up to $Re_\tau = 5300$

Technical Note: **ETSIAE /MF-0219**

Alberto Vela-Martín[†]

Miguel P. Encinar

Adrián García-Gutiérrez

Javier Jiménez

[†]albertovelam@gmail.com

Computational Fluid Mechanics
School of Aeronautics
Universidad Politécnica Madrid.

June 2019

Summary

Wall-bounded flows play an important role in numerous common applications, and have been intensively studied for over a century. However, the dynamics and structure of the logarithmic and outer regions remain controversial to this date, and understanding their mechanics is essential for the development of effective control strategies and for the construction of a complete theory of wall-bounded flows. Recently, the use of time-resolved direct numerical simulations of turbulent flows at high Reynolds numbers has proved useful to study the physics of wall-bounded turbulence, but a proper analysis of the logarithmic and outer layers requires simulations at high Reynolds numbers in large domains, making the storage of complete time series impractical. In this paper a novel low-storage method for time-resolved simulations is presented. This approach reduces the cost of storing time-resolved data by retaining only the required large and intermediate scales, taking care to keep all the variables needed to fully reconstruct the flow at the level of instantaneous filtered fields and second-order statistics. This new methodology is efficiently implemented as a new high-resolution hybrid CUDA-MPI code, which exploits the advantages of GPU co-processors on distributed memory systems, and allows running for physically meaningful times. The resulting temporally-resolved database of channel flow at up to $Re_\tau = 5300$, in large boxes for long times, is briefly introduced.

The code is available at https://github.com/albertovelam/CHANNEL_GPU.

Contents

1	Introduction	1
2	Methods	3
2.1	Simulation algorithm	3
2.2	Code and scaling	4
2.3	Enforcing boundary conditions at high Reynolds numbers	5
3	A second-order consistent, low-storage time-resolved database	6
3.1	Resolution and storage	6
3.2	Recovering the pressure and other filtered variables	7
3.3	Simulations	8
4	Conclusions	9

1 Introduction

Wall bounded flows are fundamental building blocks of many industrial and scientific applications, and developing accurate models for their prediction and control is a crucial challenge for the next decades. One fourth of the energy in advanced economies is used in transportation, and about 20% of that amount is dissipated in wall-bounded turbulent flows. Therefore, 5% of the total energy, and a disproportionate amount of the resulting CO₂ emissions, are spent that way [17]. Wall turbulence is the main contributor to aerodynamic friction, and is responsible for most of the pressure drop in internal flows such as pipelines. Its importance cannot be overemphasized for the energetic future of this century. Among wall bounded flows, channels are the simplest to simulate numerically and represent a valuable tool for the accurate study of these phenomena. Their direct numerical simulation has been for some time a basic component of their study [20, 28, 7, 13, 22].

While the behaviour of turbulence in the viscous layer near the wall has been reasonably well understood for some time [31], the dynamics of the flow farther from the wall is less clear. One of the most vexing remaining problems is the logarithmic layer that separates the near-wall and outer regions. It is in this layer that most of the velocity drop of a boundary layer takes place at high Reynolds numbers, and where the transition between the very different length-scales of turbulence in the two regions is accomplished. The logarithmic layer has been studied experimentally for a long time, but numerical simulations have only been possible in the last decade because it only exists at relatively high Reynolds numbers [16]. It is generally accepted that the logarithmic layer extends from above $yu_\tau/\nu \approx 150$ to $y/h = 0.15$ (although other limits have been proposed), where y is the distance from the wall, u_τ is the friction velocity, ν is the kinematic viscosity, and h is the boundary-layer thickness (or the channel half-width). Therefore, a logarithmic layer does not exist if the friction Reynolds number is $Re_\tau = u_\tau h/\nu \lesssim 1000$, and it is only appreciably long if Re_τ is substantially higher.

The first DNSes of a channel flow had $Re_\tau = 180$ [20], and no logarithmic layer in the sense just mentioned. Since then, Re_τ has increased steadily, and simulations with a short logarithmic layer have become available. The current state of the art is $Re_\tau \sim 4000 - 8000$ [1, 25, 22, 37], where the logarithmic layer extends over a ratio of 5 to 8 in y .

DNS has traditionally focused on producing high-quality snapshots and bulk properties of statistically steady canonical turbulent flows. In the case of channels, this is typically done in numerical boxes periodic in the two wall-parallel dimensions, and it was soon realized that the size of the numerical box is an important parameter that constrains the size of the largest ‘well-resolved’ structures [8, 25]. The computational box has to be large enough for the structures of interest to be unconstrained, in the same way as the grid has to be fine enough to capture the smallest eddies and to reproduce the correct dissipation. A *de-facto* standard for large-box simulations is $(\text{length} \times \text{span}) = (8\pi \times 3\pi)h$ [16]. Experiments, and simulations in boxes up to $(60\pi \times 6\pi)h$ [25], have shown that this is a reasonable estimate for the size of the largest structures that arise in channels. Although a lot can be gained by analysing the temporal evolution of the smaller structures in smaller boxes [26], the largest scales contain most of the total kinetic energy and Reynolds stresses (and, therefore, of the drag) of the flow, especially at high Reynolds numbers [15, 21, 6, 24, 8]. Understanding them is important.

Another reason for considering the large scales has recently become apparent. The buffer region near the wall has traditionally been considered the prime target for turbulence control, but the dimensions and frequencies involved are demanding. In a wing at transonic speeds, where $u_\tau \approx 10$ m/s and $\nu/u_\tau \approx 10^{-6}$ m, the buffer-layer structures have wall-parallel dimensions $(500 \times 100)\nu/u_\tau \approx (0.5 \times 0.1)$ mm, and approximately 10^{10} sensors and actuators would be required to control the flow over a typical 300 m² wing. Their passing frequency is 20 KHz, which generates 2×10^{14} floating point data per second. Supposing, for simplicity, 5 operations per datum to obtain the desired control, one petaflop of computing power is required for this task. An alternative is to target the structures in the logarithmic layer, whose size is about $(0.3 \times 0.1)h$. For $h \approx 2$ cm, the number of logarithmic-layer structures over a typical wing is a ‘more manageable’

10^5 , with a passing frequency of 30 Hz. However, the possibility of control of these larger scales depends on a theoretical understanding that is still missing.

The increased availability of large computers has provided turbulent channels whose small and large scales are well resolved, but dynamics require temporally resolved data. All DNSes are by definition temporally resolved while they are being computed, but the possibility of *storing* and post-processing temporally resolved time series, instead of a few independent snapshots, is more recent. After early efforts at NASA Ames and Stanford [30], our group pioneered the subsequent use of temporal series at higher Reynolds numbers, especially in wall-bounded flows [12, 25], which were then made freely available to the community [35]. These public databases marked an inflection point in turbulence research, because they allowed several groups to test hypotheses on the same data, and to refine them interactively. The limiting resource is storage space and post-processing time, and the task of storing and analysing temporally and spatially resolved time series of high-Reynolds numbers channels in large boxes is still economically challenging. Luckily, although DNS simulations have to be well resolved to reproduce the physics, large and small scales are relatively independent, and do not need to be post-processed together. Recent simulations have shown that damping [14], or even removing [27, 9] the small scales near the wall, has negligible effects on the logarithmic-layer structures, and it has been known for some time that large-eddy simulations, which have no small scales, reproduce the large structures correctly [32].

Part of the reason for the high cost of generating and storing useful temporal series of the large flow scales is that the simulation time has to be long, because these scales evolve relatively slowly and can only be studied over long time intervals. The lifetime of structures centred at a distance y from the wall is $u_\tau T \approx 6y$ [12], or about an eddy-turnover time (ETT, $T_{eto} = h/u_\tau$) for structures at $y/h = 0.15$. Reasonable statistics require $u_\tau t/h \approx 30$.

We have discussed in the previous paragraphs the importance of an adequate Reynolds number, of a large box size, and of *storing* temporally resolved and sufficiently long series of turbulent channel simulations. Reviewing the characteristics of currently available data bases, it is clear that none of them meets all these desirable properties, although some combinations of two of them can be found. For example, recent non-time-resolved simulations at high Reynolds numbers in large boxes are found in [22]. Time-resolved series at moderate Reynolds numbers ($Re_\tau = 1000$ – 2000) have been available at our group for some time [12, 25, 35], but in reduced box sizes. A more recent addition to the available data bases is [29], which includes an $Re_\tau = 1000$ time-resolved channel in a large box, although only for a relatively short period ($u_\tau t/h \approx 1.4$). While large boxes require larger computational resources than smaller ones at the same Reynolds number, both share the limiting factor of storing, sharing, and post-processing the computed data. For example, assuming a maximum data storage of 200 TB, and a target $Re_\tau = 4000$, the choice is between saving 500 snapshots of a large $(8\pi \times 3\pi)h$ box, or 6500 snapshots of a simulation in a smaller $(2\pi \times \pi)h$ box. The latter database would provide six ETT with a reasonable time interval between snapshots [26], while the former would only contain 0.5 ETT.

The storage limitations can be alleviated if one mostly wishes to study the dynamics of the large and intermediate motions which, as mentioned above, are the ones that require large boxes. This paper covers the computation and generation of a database for a state-of-the-art Reynolds number ($Re_\tau \sim 5000$) in a $(8\pi \times 3\pi)h$ box, providing time-resolved data for a reasonably long time. Storage requirements are reduced by only storing physically accurate data obtained by *a-posteriori* filtering of a DNS. Regular statistics of the fully resolved flow are computed and stored on-the-fly. With this new approach, storing a time-resolved channel simulation in a large box becomes feasible, and opens new possibilities for studying the temporal evolution of accurately computed large-scale motions in a wall-bounded flow. The downside is that the small scales are only preserved in the form of post-processed statistics, and that some quantities related to those scales are not available in a time-resolved fashion. This is justified by the availability of the time-resolved simulations mentioned above in boxes which, although smaller, are large enough to allow the small scales to be studied [12, 25, 29].

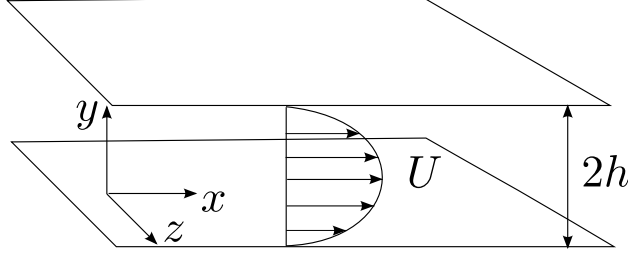


Figure 2.1: Sketch of channel flow between two parallel walls

In this work we also validate the suitability of GPUs for large-scale direct numerical simulations of turbulent flows. Although GPUs have been part of many supercomputers for some time, their use for solving fluid mechanics problems is not general. Some previous codes have made use of many GPUs to gain a considerable speed-up [19, 18], but they generally use low-resolution spatial discretisation schemes that make them less suitable for high-Reynolds number turbulence. Our results prove that the use of GPUs can also be advantageous for the computation of communication-intensive simulations such as those needed to compute turbulence with high-order schemes. For implementations that spend about 40% of the time transferring data, asynchronous overlapping between communications and computation can speed up simulations by a factor of two with respect to a standard CPU code running on the same machine. For large simulations spanning months, this advantage is crucial. As network bandwidth and clusters architecture improve, and the fraction of time spent communicating decreases, the advantage of using GPUs should be even clearer. When the next step in supercomputing is taken, and new hexascale machines become available, efficient devices will be required to keep energy consumption down to a reasonable level. GPUs have proved to be efficient and fast and are present in ever more super-computer centres, as they deliver good performance while keeping energy consumption low. The code used in this investigation takes advantage of the use of GPUs on a large scale, and represents a step into using future heterogeneous CPU/GPU hexascale architectures for DNS simulations. It is available in [3].

This paper is organized as follows. The algorithm and code employed are described in §2, with details on the running performance and of the test simulations performed. Section 3 describes the storage approach, the simulations performed for the database, the main statistics of those simulations, and their validation. Finally, conclusions are offered in §4

2 Methods

2.1 Simulation algorithm

We consider the turbulent flow between two parallel planes separated by $2h$. Both the spanwise, z , and the streamwise, x , directions are periodic, with period L_z and L_x , respectively. A constant mass flux is imposed in the streamwise direction by a time-variable mean pressure gradient. The plane-averaged velocity in the wall-normal direction, y , is zero at all distances from the wall because of incompressibility and of the impermeability condition at the wall. The mean value of the spanwise velocity component is allowed to drift, since no pressure gradient is applied along that direction, but its long-term average is non-drifting. A sketch of the flow is shown in figure 2.1. Magnitudes expressed in ‘wall’ units constructed from the friction velocity u_τ and the kinematic viscosity ν , are denoted by a ‘+’ superindex, so that $Re_\tau = h^+$. Upper case symbols are used for ensemble-average quantities, such as the mean velocity profile U , while primes are reserved for root-mean-square intensities, as in u' .

The evolution equations for the stream-wise, wall-normal and span-wise velocities, u, v and w (or u_x, u_y, u_z), respectively, are the Navier–Stokes equations for an incompressible fluid,

$$\partial_t u_i = -u_j \partial_j u_i - \partial_i p + \nu \partial_{kk} u_i, \quad (2.1)$$

	$N_x \times N_y \times N_z$	$N_{gpus}^{min} - N_{gpus}^{max}$	τ_{min} (ns)
★	$1024 \times 256 \times 1024$	16 – 256	47
+	$2048 \times 512 \times 2048$	64 – 512	48
○	$4096 \times 1024 \times 4096$	512 – 1024	58
□	$6144 \times 1024 \times 4096$	512 – 1024	54

Table 2.1: Parameters of the test cases run for the scalability analysis, where τ is the time per step and degree of freedom (see text for definition). N_{gpus}^{min} and N_{gpus}^{max} are the minimum and maximum number of GPUs in which each case has been run. N_{gpus} is always chosen a power of two.

$$\partial_i u_i = 0, \quad (2.2)$$

where p is the kinematic pressure, and repeated indices imply summation. For convenience, equations (2.1) and (2.2) are reduced to two equations for the vorticity in the wall-normal direction, ω_y , and for the Laplacian of the wall-normal velocity, $\nabla^2 v$, thus removing the computation of the pressure [20].

The equations are then projected on a Fourier basis with N_x and N_z modes in each periodic direction. Therefore, the mesh in real space is uniformly spaced with N_x and N_z collocation nodes, chosen to provide the desired resolution. Non-linear terms are computed with a pseudo-spectral method and are fully dealiased by zero padding [2]. In the wall-normal direction, the equations are discretized on a non-uniform mesh of N_y points, adjusted to keep at all wall distances an approximately constant resolution in terms of the local Kolmogorov scale [11]. Derivatives in that direction are computed on the mesh using seven-point compact finite differences with spectral-like resolution [23]. A semi-implicit third-order low-storage Runge-Kutta is used for temporal integration [34].

2.2 Code and scaling

A plane-plane decomposition is used to partition the computational domain among nodes and GPUs. A configuration in y - z planes is used to perform operations in the y direction (mostly banded-matrix solvers), where the use of compact finite difference requires local access to all points in that direction. For the computation of the non-linear convolution in the wall-parallel planes, the domain is reorganised in x - z planes in order to apply direct and inverse Fourier transforms, using CUFFT [5]. All the transpose operations are performed using custom CUDA kernels to take advantage of the high memory bandwidth of the GPUs. Several strategies are used for the MPI communication part, from all-to-all to send/receive. Particular care is taken to overlap as much as possible communications and computations. This is done using three GPU streams: one for computation and two for device-host/host-device communications. Appropriate care is taken to optimize the CUDA kernels as much as possible.

The scaling of the code has been tested for cases ranging from small ones used for code validation, to a case equivalent to the largest simulation performed. All cases tested have a grid ($N_x \times N_y \times N_z$) with an aspect ratio similar to the production run, to keep performance comparable. The maximum and minimum number of GPUs used to run each case is limited by code design and by GPU memory. The domain decomposition is intended to exploit maximum GPU occupancy and minimum global communications. The plane-plane decomposition mentioned above constrains the maximum number of GPUs on which the code can run to the number of points in y . When both numbers coincide, a single x - z plane is processed per GPU. On the other hand, the minimum number of GPUs required is constrained by the memory of each GPU. The code has been tailored to achieve maximum speed while keeping memory consumption low enough to run large cases in a reasonable number of GPUs. A summary of test cases is presented in table 2.2.

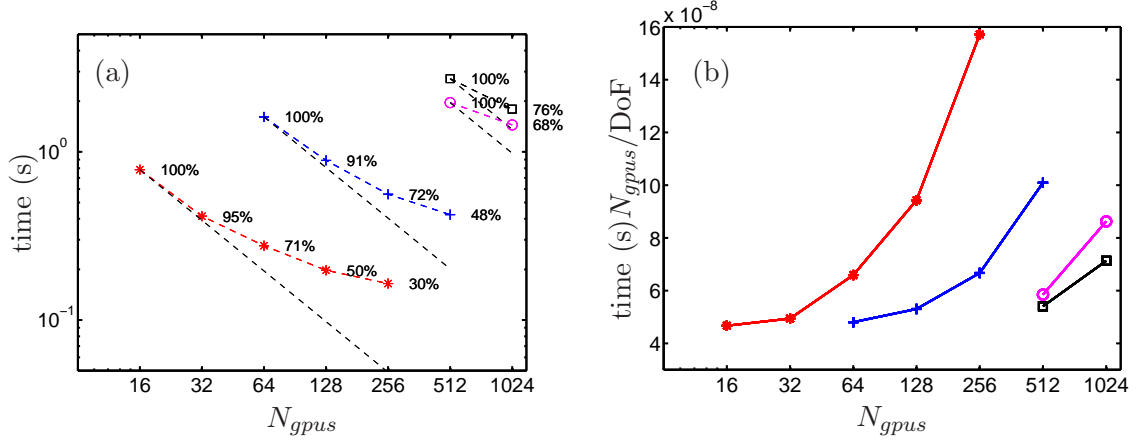


Figure 2.2: (a) Execution time per step (seconds) as a function of the number of GPUs for different test cases. Percentages represent efficiency, t/t_{ideal} . (b) Total execution time per time step and per degree of freedom.

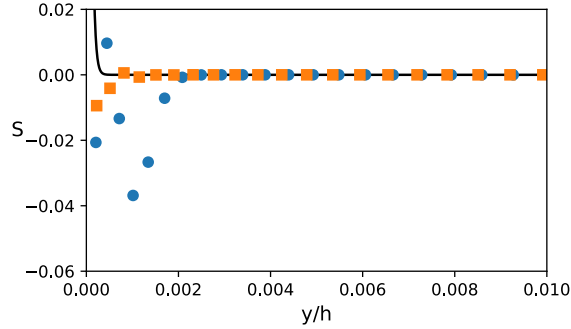


Figure 2.3: Solution of the Helmholtz equation for the most critical wavenumber. — Analytic solution. ●, standard mesh; ■, optimized mesh.

Results of the scaling tests conducted in PizDaint, a GPU-based supercomputer part of the PRACE Tier-0 network [4], are shown in figure 2.2. Efficiency is defined as t/t_{ideal} where t is the execution time per RK3 step in N_{gpus} GPUs, and $t_{ideal} = t_0 N_0 / N_{gpus}$ is the ideal expected time, where N_0 is the minimum number of GPUs that can be used for a particular grid size, determined by the GPU memory, and t_0 is the execution time for that case. The total time spent per RK3 step and degree of freedom (DoF), $\tau = t N_{gpus} / \text{DoF}$, is compared in figure 2.2(b) for all test cases. Table 2.2 compares the minimum τ for each case, showing the good scalability properties of the code. These scaling results prove the suitability of the code for simulations in large high-performance computing facilities. The speed-up obtained by using GPUs allows us to run simulations for longer times than with typical CPU codes.

2.3 Enforcing boundary conditions at high Reynolds numbers

The use of high-order, high-resolution numerical approximations for the derivatives in the wall-normal direction is essential in turbulent channel DNSes. However these methods are prone to numerical errors if they are not developed together with the mesh. The most numerically sensitive operation in the vorticity–Laplacian formulation of the Navier–Stokes equations is the solution of the bilaplacian operator [20], which requires the solution of multiple homogeneous Helmholtz equations to impose the boundary conditions. For high Reynolds numbers and small wavelengths, these solutions include very thin boundary layers near the wall, and we found important numerical errors in the homogeneous solutions when compact finite differences of up to twelfth order of consistency are used for the discretisation of the second derivative.

Figure 2.3 compares the worst-case solution for the Helmholtz problem used in the simulation (the one with the highest wavenumbers). The grid spacing of the original mesh, represented in the figure by circles, are optimized considering only physical arguments, as in [13]. This mesh worked well with low-order schemes, but the wide stencils used here led to large errors in the first few grid points, which, in extreme cases, were enough to make the simulation unstable. A refined mesh, plotted in squares, solved the problem of code instability by slightly displacing the first 20 grid points in order to minimize the error of the most dangerous solutions without affecting too much the individual grid spacing, thus preserving the physical properties of the mesh.

3 A second-order consistent, low-storage time-resolved database

3.1 Resolution and storage

From previous experience [26, 29], storing the time-resolved evolution of all the flow scales in a turbulent channel simulation at $Re_\tau \sim 5000$, spanning 30 ETT in a $(8\pi \times 3\pi)h$ box, would require 60 PB of data. However, most of the information in those data sets represents the dynamics of viscous scales, which can be more efficiently studied using smaller simulation boxes requiring much less computational effort and storage space.

As a consequence, our database only *stores* scales above the viscous limit, even if the computation is performed at full resolution. This reduces the storage requirements by three orders of magnitude, because of the lower spatial and temporal resolution required to accurately capture the dynamics of the larger scales. If we wish to discard the dissipative eddies, the inertial range can be estimated to start above approximately 50η [16], where η is the Kolmogorov length-scale, roughly equivalent to 100 wall units. Thus, we only retain eddies with size $l_e^+ > 100$. To be able to track them in time as they are advected with velocity u_e , the characteristic time, Δt_e , between snapshots should not be larger than l_e/u_e . This advection velocity can be measured in any convenient frame of reference, which may be a function of y [26]. It is most economical to choose as reference the local mean flow, so that advection is only due to the fluctuations, $u_e \approx u'$. The most restrictive condition is due to the streamwise velocity perturbations, which are $u'^+ \sim 2$ in the logarithmic layer, so that $\Delta t_e^+ \lesssim 100/2 \approx 50$. This implies storing approximately $N_{ETT} = Re_\tau/\Delta t_e^+$ snapshots per ETT, or $N_{ETT} \approx 100$ in the case of F5000.

In practice, the velocity fields are filtered to retain scales above $l_{ex}^+ \sim 100$ in x and $l_{ez}^+ \sim 50$ in z , and stored with the aforementioned temporal resolution. At that resolution, the number of storage points required for an $(8\pi \times 3\pi)h$ box at $Re_\tau \sim 5000$ are $M_x = L_x/l_{ex} \sim 1250$ along x , and $M_z = L_z/l_{ez} \sim 950$ along z . The effect of the removed scales on the larger ones is not negligible, and it is impossible to recover from the filtered velocities alone, posing a considerable limitation to what could be studied and computed from the stored data. To partially overcome it, we also store all the components of the filtered Reynolds-stress tensor, $u_i u_j$, which are second-order non-linear quantities appearing in the filtered equations of motion. From the six filtered Reynolds stresses, the effect of the small scales on the dynamics the filtered ones can be reconstructed, preserving their correct temporal derivatives, and all the sub-grid quantities required for a-priori testing of large-eddy simulations (LES). In particular, the filtered pressure is an important quantity, but we will see below that it can be retrieved from the filtered velocities and from the Reynolds-stress tensor. Lastly, we also store the filtered enstrophy, which is often used in characterising turbulence.

Moreover, as stated before, our interest resides in the largest flow scales, making the resolution of the very-small scales not a key factor in our simulations, at least as long as the dynamics of the large scales are unaffected. Recent experiments with DNS of turbulent boundary layers (Ayse G. Gungor, private communication) show that it is possible to degrade the resolution in the wall-parallel directions by a factor of two without significantly affecting the large-scale energy spectrum. In figure 3.1, the velocity spectra at high ($\Delta x^+ = 6$ and $\Delta z^+ = 4$) and low ($\Delta x^+ = 24$ and $\Delta z^+ = 9$) resolution are shown to be similar despite large differences in the grid. Guided by these results, we slightly lowered the resolution of our simulations in the stream- and span-wise

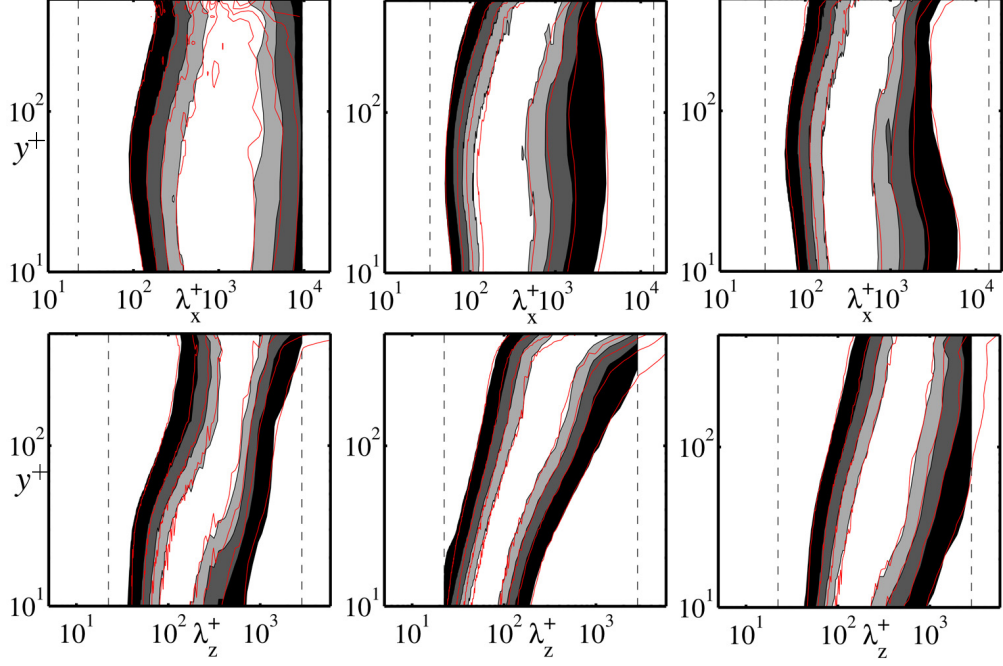


Figure 3.1: Spectra of a turbulent boundary layer as a function of the distance from the wall. The three velocity components, (u, v, w) , are shown from left to right. Red lines correspond to a full-resolution simulation ($\Delta x^+ = 12$ and $\Delta z^+ = 6$), and shaded contours to a simulation on a coarser grid ($\Delta x^+ = 18$ and $\Delta z^+ = 9$). The dashed vertical lines mark the resolution of the grid and the size of the box of the coarser simulation. Boundary layer at from $Re_\tau \approx 510$ (data courtesy of Ayse G. Gungor, private communication).

directions, allowing us to run longer flow times at the same cost. Adopting $\Delta x^+ = 20$ and $\Delta z^+ = 10$ for a simulation at $Re_\tau \sim 5000$ in a $(8\pi \times 3\pi)h$ box, we obtain $N_x = L_x Re_\tau / \Delta x^+ \sim 6144$, and $N_z = L_z Re_\tau / \Delta z^+ \sim 4096$. The resolution in the wall-normal direction is only reduced by 15% with respect to the standard, to $N_y = 1024$, and is not further reduced for storage.

3.2 Recovering the pressure and other filtered variables

We choose a sharp Fourier cutoff in the wall-parallel directions as the database filter. Although the spectral properties of this filter are not necessarily ‘good’, it commutes with all the derivatives, and allows us to perform linear operations on the stored quantities without requiring extra information from the small scales. The ten variables in the database are $\overline{u_i}$, $\overline{u_i u_j}$, $\overline{\omega_i \omega_i}$, where $\overline{(\cdot)}$ denotes cutoff filtering and repeated indices imply summation. Some of the ‘derived’ variables that can trivially be computed from the database are the filtered rate-of-strain tensor, the kinetic energy, $\overline{E} = \frac{1}{2} \overline{u_i u_i}$, and the filtered vorticities, $\overline{\omega_i} = \varepsilon_{ijk} \partial_j \overline{u_k}$, where ε_{ijk} is the fully antisymmetric Levi-Civita symbol. The computation of the pressure is less evident, but equally possible. Taking the divergence of the momentum equation and using continuity yields,

$$\partial_{kk} p = -\partial_{ij} (u_i u_j). \quad (3.1)$$

This is the well-known Poisson equation for the pressure, and is linear in p and $u_i u_j$. Therefore,

$$\partial_{kk} \overline{p} = -\partial_{ij} (\overline{u_i u_j}), \quad (3.2)$$

which requires only the cross-derivatives of the filtered Reynolds stress tensor in the database. An identity worth noting is,

$$-2\partial_{ij} (\overline{u_i u_j}) = \overline{S_{ij} S_{ij}} - \overline{\omega_i \omega_i}, \quad (3.3)$$

<i>Name</i>	Re_τ	L_x/h	L_z/h	$N_x \times N_y \times N_z$	$M_x \times M_y \times M_z$	t/T_{eto}	N_{snap}
F2000	2000	8π	3π	$2048 \times 512 \times 2048$	$512 \times 512 \times 512$	14	1300
F5000	5303	8π	3π	$6144 \times 1024 \times 4096$	$1024 \times 1024 \times 1024$	36	3900
L2000	2003	8π	3π	$4096 \times 633 \times 3072$	—	10	232
L5000	5200	8π	3π	$10240 \times 1536 \times 7680$	—	7.8	—

Table 3.1: New simulations in the database (F2000 and F5000), and simulations used to validate them (L2000 [13] and L5000 [22]). N_i is the simulation resolution, and M_i is the storing resolution. t/T_{eto} is the simulation time in eddy-turnovers, and N_{snap} is the number of snapshots available in the database.

which allows us to compute the norm of the rate-of-strain tensor from the filtered enstrophy and the right hand side of the filtered pressure equation.

Finally, the availability of a closed second-order database can be useful for a-priori testing of LES models at high Reynolds numbers. The sub-grid stress tensor can be computed from the filtered velocities as,

$$\tau_{ij} = \overline{u_i u_j} - \bar{u}_i \bar{u}_j, \quad (3.4)$$

providing time-resolved information on the quantities that LES models are intended to represent.

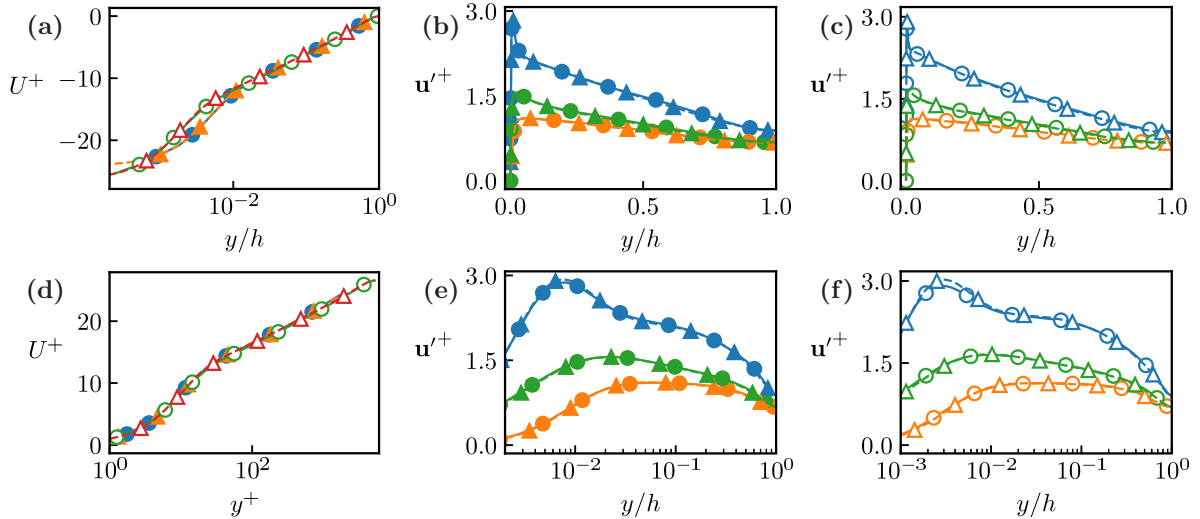


Figure 3.2: Mean and fluctuation velocity profiles for the simulations in table 3.1. Symbols are: triangles for the reference simulations, and circles for the new ones. Closed symbols are $Re_\tau = 2000$, and open ones are $Re_\tau = 5200$. (a) Mean velocity profile in velocity-defect form for all the simulations. (b) Fluctuation velocity intensities for simulations at $Re_\tau = 2000$. (c) As in (b), for $Re_\tau = 5200$. (d) Mean velocity profile plotted in wall units, for all the simulations. (e) Fluctuation velocity intensities for simulations at $Re_\tau = 2000$, emphasizing the near-wall region. (f) As in (e), for $Re_\tau = 5200$.

3.3 Simulations

Table 3.1 summarizes the new simulations in the database, as well as the older ones used for validating them. The new simulations ran in PizDaint for a total of 65000 node-hours on 128 GPUs in the case of F2000, and 1.4 million node-hours on 512 GPUs in the case of F5000. The size of the filtered databases is 5.6 TB and 150 TB, respectively. The initial conditions were interpolated from a lower Reynolds number equilibrium simulation (L2000), and the first five ETT immediately after the initial interpolation were discarded in each case.

Figure 3.2 shows the main one-point statistics of the simulations in table 3.1. The mean velocity profiles follow the ones of the full-resolution simulations across the whole channel, and collapse as expected, both in inner and in outer units. The fluctuation velocities also agree everywhere, except in the vicinity of the peak of u' , where some perturbation energy is missing from the new simulations. This disparity may be Reynolds-number dependent, although the slight disparities in resolution and Reynolds number among the simulations make this conclusion uncertain. It is not present in simulations performed with similar differences in resolution at $Re_\tau = 1000$ (not shown), but u'^2 lacks about 1% from its peak in F2000, and the effect is most pronounced in F5000, where the energy difference is 3%. The effect seems to be related to the resolution in the stream- and span-wise directions. Tests carried with a higher-resolution mesh in the wall-normal direction discarded the grid-spacing in y as the principal cause for the disparity. Nevertheless, the regions in the logarithmic-layer, $y^+ \gtrsim 100$, which are the principal object of our study, show healthy statistics for the three velocity components at the two Reynolds numbers in the database.

The spectra of the three velocity components are displayed in figure 3.3 at $y^+ = 150$. This is the lower end of the logarithmic layer, where the energy tends to be concentrated at the smallest scales and therefore where the lower resolution of the database simulations could be most critical. The spectra of the new simulations collapse well with the reference ones over all the scales retained by the filter. As expected, the wall-normal velocity component is the one worst retained in the filtered database, with approximately 20% of the energy of F5000 lost in filtering. On the contrary, the stream- and span-wise velocities retain more than 90% and 95% of their energy, respectively. As with the one-point statistics, there is no indication that the lower resolution of the simulation affects in any important way the stored turbulence data, which agree well with fully resolved simulations.

Figure 3.4(a) shows the temporal evolution of the instantaneous friction velocity u_τ in the bottom wall, across approximately 25 ETT. The largest variations of the value of u_τ have a slow characteristic time, while the changes that it experiences over times smaller than one ETT are smaller. The largest differences in the value of u_τ within time windows of one ETT are approximately 5 times smaller than those within 10 ETT. This implies that structures with lifetimes longer than one ETT are present in the flow, and contribute to the shear stress at the wall. Further insight can be gained from the premultiplied temporal spectra of this signal, shown in figure 3.4(b), computed by smoothly windowing the temporal signal to prevent its lack of periodicity from harming the spectrum [36]. Approximately, 34% of the spectral mass, and thus of the skin friction fluctuations, is contained in periods longer than one ETT. Figure 3.4(c) shows the z - t spectrum of several streamwise Fourier modes at $y/h = 0.4$, which is the distance from the wall where the streamwise velocity structures are longest [16]. The two longest streamwise modes have characteristic times longer than one eddy turnover, independently of their spanwise wavelength. Most of the energy of the infinitely long streamwise streaks, represented by the $k_x = 0$ wavenumber, is contained in lifetimes longer than 6 ETT. These structures have a typical width of $\lambda_z/h \approx 2 - 3$, wider than the typical size of the outer-layer streaks [33]. The structures represented by the modes with $\lambda_x/h = 8\pi$ can be thought of as streamwise velocity streaks with length of approximately $12h$ and width $1.5h$, and have much shorter lifetimes, peaking at $Tu_\tau/h = 1 - 2$.

4 Conclusions

We have presented a new data base of turbulent channel flows containing time-resolved simulations at $Re_\tau = 2000$ and $Re_\tau = 5000$, for long times $tu_\tau/h \sim 30$, in large boxes of size $(8\pi \times 3\pi)h$. With a traditional resolution in time and space, storage size becomes the limiting factor. In the present case, it would require approximately 60 PB. To alleviate these requirements, and since the database is mainly intended to study the relatively large scales of the logarithmic layer, we only store structures filtered above the viscous limit, even if the simulation runs at full resolution. On the other hand, the data include the long histories required to capture the large-scale dynamics. To capture the influence of the discarded scales on the stored ones, the database also includes

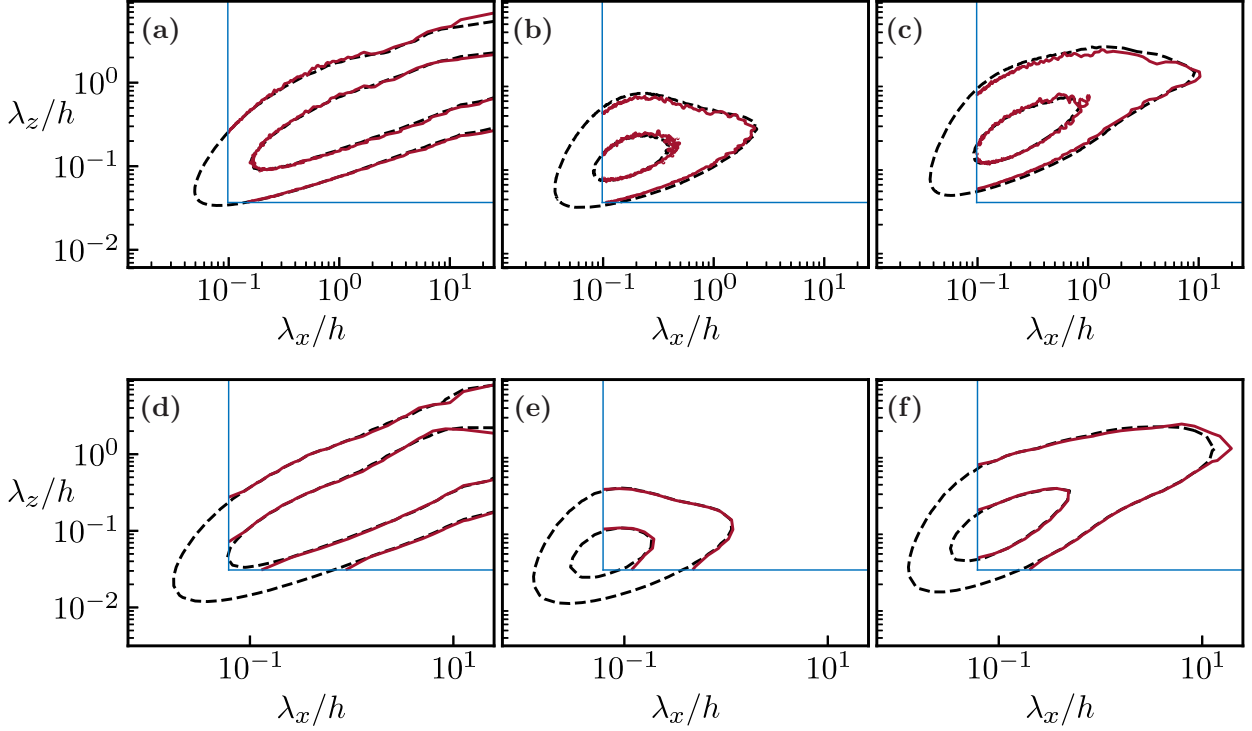


Figure 3.3: Spectra of the velocity components at $y^+ = 150$ for the simulations in table 2.2. (a-c) Spectra of u, v, w for L2000 (dashed line) and F2000 (solid red line). (d-f) As in (a-c), for L5000 and F5000. Contours contain 50% and 10% of the spectral mass. The thin rectangle marks the database resolution in all cases.

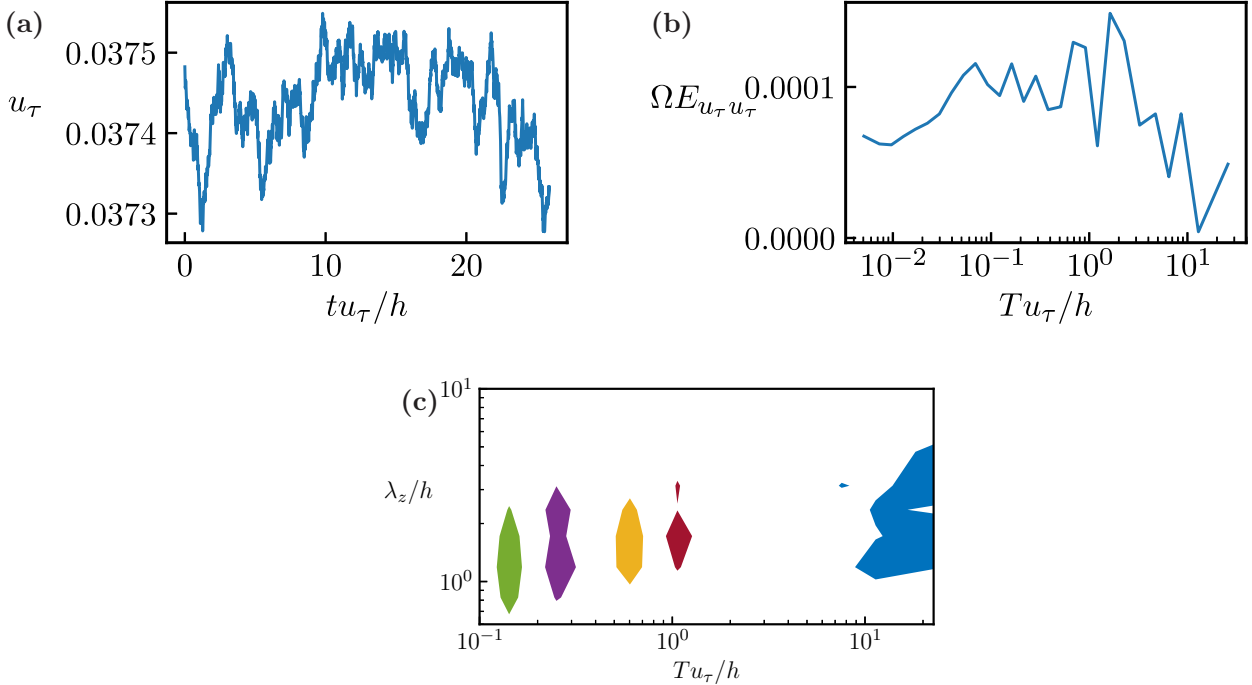


Figure 3.4: (a) Time evolution of the friction velocity at the bottom wall. (b) Premultiplied temporal spectrum of the signal in (a). (c) Premultiplied $(z-t)$ spectra for the first few streamwise Fourier modes of u at $y/h = 0.4$. From right to left, $\lambda_x = \infty$ (blue), $\lambda_x/h = 8\pi$ (red), $\lambda_x/h = 4\pi$ (yellow), $\lambda_x/h = 2\pi$ (purple), $\lambda_x/h = \pi$ (green). The contour is 40% of the maximum for each streamwise wavelength. F5000.

the instantaneous filtered Reynolds-stress tensor and the filtered enstrophy . This is still more economical than storing the full flow fields (~ 150 TB), and allows the reconstruction of other quantities of interest, such as the time derivatives of the filtered velocities, the filtered pressure, and the filtered norm of the rate-of-strain tensor. In this sense, the database is ‘second order consistent’, because any observable that depends on quadratic velocity products can be computed a posteriori. In particular, this property, together with relatively high Reynolds numbers, makes the database potentially useful for a-priori testing and development of new LES models.

In order to achieve the required running times, we employ a novel code which runs on many distributed GPUs and takes advantage of their highly efficient and powerful architectures. We show that this code scales up to 1024 GPUs, proving its suitability for the next generation of heterogeneous hexascale computers.

To further reduce the cost of the simulations we slightly degrade the resolution of the computational grid, but we show that the first- and second-order, one- and two-point statistics of the retained scales are not affected by this resolution change, and that we generate ‘healthy’ logarithmic and outer regions.

From a preliminary analysis of the data, we show that time scales longer than one eddy-turnover time are present in the channel flow, especially for the streamwise velocity component. Some of these structures, responsible for about one third of the variation in the total turbulent skin friction, have characteristic times of $tu_\tau/h \approx 6$. The same is true of the longest structures of u , but the long simulations make the study of their dynamics possible. A more detailed study of the flow properties can be found in [10].

Acknowledgments

This work was supported by the COTURB project of the European Research Council (ERC2014.AdG-669505). The new simulations ran in PizDaint under the PRACE Tier-0 project TREC. We are grateful to A.G. Gungor, for providing the data in figure 3.1, and to M. Fatica and E. Phillips, from Nvidia, for invaluable help in optimizing the performance of the GPU CUDA code.

References

- [1] M. Bernardini, S. Pirozzoli, and P. Orlandi. Velocity statistics in turbulent channel flow up to $Re_\tau = 4000$. *J. Fluid Mech.*, 742:171–191, 2014.
- [2] C. Canuto, M. Y. Hussaini, A. Quarteroni, and T. A. Zang. *Spectral Methods in Fluid Dynamics*. Springer-Verlag, Heidelberg, 1988.
- [3] https://github.com/albertovelam/CHANNEL_GPU.
- [4] <https://www.cscs.ch/>.
- [5] <https://docs.nvidia.com/cuda/cufft/index.html>.
- [6] J. C. del Álamo and J. Jiménez. Direct numerical simulation of the very large anisotropic scales in a turbulent channel. In *CTR Ann. Res. Briefs*, pages 329 – 341. Stanford U., 2001.
- [7] J. C. del Álamo and J. Jiménez. Spectra of the very large anisotropic scales in turbulent channels. *Phys. Fluids A*, 15:L41 – L44, 2003.
- [8] J. C. del Álamo, J. Jiménez, P. Zandonade, and R. D. Moser. Scaling of the energy spectra of turbulent channels. *J. Fluid Mech.*, 500:135–144, 2004.
- [9] S. Dong, A. Lozano-Durán, A. Sekimoto, and J. Jiménez. Coherent structures in statistically stationary homogeneous shear turbulence. *J. Fluid Mech.*, 816:167–208, 2017.

- [10] M. P. Encinar, A. Vela-Martín, and J. Jiménez. Spatio-temporal statistics of the large turbulent scales in channels up to $Re_\tau = 5300$. *Submitted*, 2019.
- [11] O. Flores and J. Jiménez. Effect of wall-boundary disturbances on turbulent channel flows. *J. Fluid Mech.*, 566:357–376, 2006.
- [12] O. Flores and J. Jiménez. Hierarchy of minimal flow units in the logarithmic layer. *Phys. Fluids*, 22:071704, 2010.
- [13] S. Hoyas and J. Jiménez. Scaling of the velocity fluctuations in turbulent channels up to $Re_\tau = 2003$. *Phys. Fluids*, 18:011702, 2006.
- [14] Y. Hwang and C. Cossu. Self-sustained processes in the logarithmic layer of turbulent channel flows. *Phys. Fluids*, 23:061702, 2011.
- [15] J. Jiménez. The largest scales of turbulence. In *CTR Ann. Res. Briefs*, pages 137–154. Stanford U., 1998.
- [16] J. Jiménez. Cascades in wall-bounded turbulence. *Ann. Rev. Fluid Mech.*, 44:27–45, 2012.
- [17] J. Jiménez. Near-wall turbulence. *Phys. Fluids*, 25:101302, 2013.
- [18] K. I. Karantasis, E. D. Polychronopoulos, and J. A. Ekaterinaris. High-order accurate simulation of compressible flows on GPU clusters over software distributed shared memory. *Comput. Fluids*, 93:18–29, 2014.
- [19] A. Khajeh-Saeed and J. B. Perot. Direct numerical simulation of turbulence using GPU accelerated supercomputers. *J. Comput. Phys.*, 235:241–257, 2013.
- [20] J. Kim, P. Moin, and R. D. Moser. Turbulence statistics in fully developed channel flow at low Reynolds number. *J. Fluid Mech.*, 177:133–166, 1987.
- [21] K. Kim and R. J. Adrian. Very-large-scale motion in the outer layer. *Phys. Fluids*, pages 417–422, 1999.
- [22] M. Lee and R. D. Moser. Direct numerical simulation of turbulent channel flow up to $Re_\tau \approx 5200$. *J. Fluid Mech.*, 774:395–415, 2015.
- [23] S. K. Lele. Compact finite difference schemes with spectral-like resolution. *J. Comput. Phys.*, 103:16–42, 1992.
- [24] Z. Liu, R. J. Adrian, and T. J. Hanratty. Large-scale modes of turbulent channel flow: transport and structure. *J. Fluid Mech.*, 448:53 – 80, 2001.
- [25] A. Lozano-Durán and J. Jiménez. Effect of the computational domain on direct simulations of turbulent channels up to $Re_\tau = 4200$. *Phys. Fluids*, 26:011702, 2014.
- [26] A. Lozano-Durán and J. Jiménez. Time-resolved evolution of coherent structures in turbulent channels: characterization of eddies and cascades. *J. Fluid Mech.*, 759:432–471, 2014.
- [27] Y. Mizuno and J. Jiménez. Wall turbulence without walls. *J. Fluid Mech.*, 723:429–455, 2013.
- [28] R. D. Moser, J. Kim, and N. N. Mansour. Direct numerical simulation of turbulent channel flow up to $Re_\tau = 590$. *Phys. Fluids*, 11:943–945, 1999.
- [29] E. Perlman, R. Burns, Y. Li, and C. Meneveau. Data exploration of turbulence simulations using a database cluster. In *Proc. SC07*, pages 23.1–23.11. ACM, New York, 2007. <http://turbulence.pha.jhu.edu>.

- [30] S. K. Robinson. Coherent motions in the turbulent boundary layer. *Ann. Rev. Fluid Mech.*, 23:601–639, 1991.
- [31] W. Schoppa and F. Hussain. Coherent structure generation in near-wall turbulence. *J. Fluid Mech.*, 453:57–108, 2002.
- [32] G. Scovazzi, J. Jiménez, and P. Moin. LES of the very large scales in a $Re_\tau = 920$ channel. In *Proc. Div. Fluid Dyn.*, pages KF–5. Am. Phys. Soc., 2001.
- [33] J. A. Sillero, J. Jiménez, and R. D. Moser. Two-point statistics for turbulent boundary layers and channels at Reynolds numbers up to $\delta^+ \approx 2000$. *Phys. Fluids*, 26:105109, 2014.
- [34] P. R. Spalart, R. D. Moser, and M. M. Rogers. Spectral methods for the Navier–Stokes equations with one infinite and two periodic directions. *J. Comput. Phys.*, 96:297–324, 1991.
- [35] <https://torroja.dmt.upm.es/turbdata/>.
- [36] P. D. Welch. The use of fast Fourier transform for the estimation of power spectra: a method based on time averaging over short modified periodograms. *IEEE Trans. Audio Electroacoust.*, 15:70–73, 1967.
- [37] Y. Yamamoto and Y. Tsuji. Numerical evidence of logarithmic regions in channel flow at $Re_\tau = 8000$. *Phys. Rev. Fluids*, 3:012602, 2018.